A tunable closed form model for the structure function of tropospheric delay

Merryman Boncori, John Peter; Mohr, Johan Jacob

Published in:
I E E E Geoscience and Remote Sensing Letters

Link to article, DOI:
10.1109/LGRS.2008.915738

Publication date:
2008

Document Version
Publisher's PDF, also known as Version of record

A Tunable Closed-Form Model for the Structure Function of Tropospheric Delay

J. P. Merryman Boncori and J. J. Mohr

***Abstract*—Several interferometric synthetic aperture radar applications could benefit from the availability of a closed-form model for the second-order statistics of atmospheric delay. Due to the variability of the latter, it would also be desirable for the model to be tunable to some acquisition-specific information, describing the atmospheric state. In this letter, a closed-form expression for the zenith delay structure function of tropospheric propagation delay is derived from a two-regime power spectral density function reported in the literature. The power at a specific spatial frequency is used as a free model parameter, which may be tuned to available measurements or, in the absence of these, to atmospheric statistics. The latter approach is used to compare the derived model with previously published results.**

***Index Terms*—Atmospheric propagation delay, statistical modeling, synthetic aperture radar (SAR) interferometry.**

I. Introduction

ONE OF the most relevant error sources in repeat-pass synthetic aperture radar (SAR) interferometry is space-time fluctuation of the atmospheric refractive index. Given the current state of the art, several applications elicit interest for a closed-form model of the second-order statistics of this disturbance.

First, as far as height and displacement measurements are concerned, atmospheric error prediction is currently only feasible within multiinterferogram frameworks. However, applications exist, such as ice-surface velocity measurement, in which only a minimum number of interferograms may be exploited due to limitations in data availability, temporal decorrelation constraints, and dynamics of the observed process itself. An error estimate may be provided also for these reduced data sets, exploiting models for the second-order statistics of error sources. A mathematical framework to do so is presented in [1, p. 61], whereas a different method based on a similar concept is detailed in [2].

Second, within multiinterferogram frameworks, second-order error statistics may be used in the data-selection process in order to ensure achievement of a desired sensitivity to the geophysical parameter of interest [3].

Finally, some recent studies have addressed the problem of atmospheric error correction, using systems other than SAR, namely, Global Positioning System [4] and satellite-imaging spectrometers [5], [6]. These studies elicit interest for statistical error modeling, since external measurements are typically available on a sparse grid as compared to interferometric SAR measurements so that some form of interpolation is required. Preliminary results indicate statistical interpolators to be the most effective for this task, and these typically exploit models of the second-order statistics of the error source [7].

In this letter, the statistical characterization of tropospheric delay through the structure function and power spectral density (PSD) modeling approaches is recalled in Section II. The underlying assumptions are discussed, and the linking equations are reported. A closed-form expression for the zenith atmospheric delay structure function is derived in Section III from a two-regime PSD function reported in literature. In Section IV, the derived model is compared to previously published results, tuning its free parameters to globally representative atmospheric statistics. The conclusions are drawn in Section V.

II. Statistical-Modelling Approaches

In the following, modeling of the propagation delay due to variations in the spatial distribution of tropospheric water vapor shall be considered. The effects of ionosphere and of changes in the vertical stratification of tropospheric refractive index may not be neglected in general, although they shall be addressed in future studies.

A. Refractivity and Delay Structure Functions

In several researches, statistical modeling of water-vapor fluctuations has been based upon the structure function of atmospheric refractivity (1). The latter is defined as $N = 10^6 \cdot (n-1)$, where n is the atmospheric refractive index

$$D_N(\vec{r}, \vec{R}) = \mathrm{E}\left[\left(N(\vec{r}+\vec{R}) - N(\vec{r})\right)^2\right]. \tag{1}$$

In (1), $\vec{r}$ and $\vec{R}$ represent the 3-D position and displacement vector, respectively, and the expected value is taken over all possible atmospheric states.

Considering the wave propagation between the radar and a point on the Earth's surface, the quantity of interest is wavefront delay, which results from integration of the refractivity field along the line of sight (geometrical-optics approximation) and is, therefore, a 2-D quantity. In the following, the one-way zenith delay (or zenith excess path length) shall be indicated with τ, and its units shall be in meters. In several independent studies [1], [10], [11], the following two regime power law for

Manuscript received April 12, 2007; revised September 15, 2007. The work of J. P. Merryman Boncori was supported by a grant from the Geoinformation Ph.D. Course, University of Rome "Tor Vergata."

The authors are with the Technical University of Denmark, 2800 Kgs. Lyngby, Denmark (e-mail: jme@oersted.dtu.dk).

Digital Object Identifier 10.1109/LGRS.2008.915738

$D_\tau(R)$ has been observed, and a third "saturation" regime is conjectured based on physical constraints

$$D_\tau(R) = \begin{cases} C_l^2 R^{5/3}, & L_0 \ll R \ll L_1 \\ C_L^2 R^{2/3}, & L_1 \ll R \ll L_2 \\ C_L^2 L_2^{2/3}, & R \gg L_2. \end{cases} \quad (2)$$

In (2), R represents horizontal distance, L_0 is the inner scale of dissipation, L_1 is the outer scale of injection, and L_2 is the saturation scale length. Finally, C_l and C_L are the structure constants of the turbulence. Functional dependence on R requires the hypothesis of homogeneity (wide-sense stationarity) and isotropy (circular symmetry).

It is agreed among the aforementioned studies that the first regime corresponds to a 3-D Kolmogorov turbulence [8], and L_1 should be on the order of a few kilometers. L_0 is instead on the order of millimeters [10] and is, therefore, not relevant for current SAR interferometers. For the second regime, it has been observed in [10] that everything goes as if Kolmogorov's "2/3 law," describing isotropic turbulence, could be extended also to scales larger than the tropospheric thickness, provided that turbulent motion is considered as 2-D in character. This interpretation is also currently accepted by other authors [12] and implies proportionality between the delay and the refractivity structure functions through the square of the effective tropospheric height. This fact is relevant for the present discussion and shall be referred to in Section III-B. Finally, for even larger scales, on the order of several hundred kilometers, the structure function is bound to "saturate"; otherwise, it would represent an infinite variance of the long-term atmospheric disturbance [11]. What happens physically at the transitions between regimes in (2) is not clear [9]. Furthermore, as far as modeling is concerned, very different values have been proposed for L_1 and L_2.

B. PSD of Phase Artifacts

A more recently proposed approach to the modeling of atmospheric artifacts in SAR interferometry is through the PSD of the phase variation associated to the excess path length. Considering two-way propagation along the zenith direction, the radar-wave's phase φ is related to the one-way zenith delay τ by

$$\varphi = \frac{4\pi}{\lambda} \cdot \tau. \quad (3)$$

It is convenient to define the PSD of φ through its autocovariance function

$$C_\varphi(\vec{r}, \vec{R}) = \mathrm{E}\left[(\varphi(\vec{r}) - \mu_\varphi) \left(\varphi(\vec{r} + \vec{R}) - \mu_\varphi \right) \right]. \quad (4)$$

In (4), $\vec{r}$ and $\vec{R}$ represent the 2-D position and displacement vector, respectively, whereas μ_φ represents the mean of φ and will be assumed zero in the following. The PSD of φ is found as the Fourier transform of $C_\varphi(\vec{r}, \vec{R})$, which, assuming wide-sense stationarity and circular symmetry, reduces to $C_\varphi(R)$, where $R = |\vec{R}|$. The one-sided PSD of φ may therefore be computed through

$$P_\varphi(f) = \begin{cases} 0, & f < 0 \\ 4 \int_0^{+\infty} C_\varphi(R) \cos(2\pi f R) dR, & f \geq 0 \end{cases} \quad (5)$$

where f represents spatial frequency.

In order to link PSD and structure function models, it is, first of all, noted that (5) holds also between the zenith delay PSD and its autocovariance, respectively, due to (3). Second, stationarity implies that the variance of the atmospheric delay $\mathrm{Var}\{\tau\}$ is assumed constant at every point in its 2-D space. Furthermore, under the hypotheses of stationarity and zero-mean, the one-way zenith delay autocovariance function may be related to the corresponding structure function through

$$C_\tau(R) = \mathrm{Var}\{\tau\} - \frac{D_\tau(R)}{2}. \quad (6)$$

In [11], a notation convention is introduced, by which the symbol $D_\tau(\infty)$ is used to represent the delay structure function value at a distance at which delay observations are uncorrelated. From (6), it follows that $D_\tau(\infty) = 2\mathrm{Var}\{\tau\}$ and thus

$$C_\tau(R) = \frac{1}{2} \left(D_\infty(R) - D_\tau(R) \right). \quad (7)$$

The autocovariance $C_\varphi(R)$ is found by taking the inverse Fourier transform of the two-sided PSD, which, by using (6) and (3), leads to

$$D_\tau(R) = \left(\frac{\lambda}{4\pi} \right)^2 \int_0^\infty 4 \sin^2(\pi f R) P_\varphi(f) df \quad (8)$$

(see also [1, p. 274]). Equations (5), (7), and (8) analytically relate the PSD and the second-order statistic modeling.

The convenience of PSD modeling lies in the fact that the disturbances on SAR phase caused by a variety of weather conditions, from thunderstorms to clear sky, were found to comply to a similar two-regime model [1], [14]. Based on [13], [1, p. 146], the following closed form may be written:

$$P_\varphi(f) = \begin{cases} (h f_0) P_0 \left(\frac{f}{f_0} \right)^{-5/3}, & \frac{1}{R_{\max}} < f \leq \frac{1}{h} \\ P_0 \left(\frac{f}{f_0} \right)^{-8/3}, & \frac{1}{h} < f \leq \frac{f_\mathrm{s}}{2} \end{cases} \quad (9)$$

where h represents the effective tropospheric height, f_0 is an arbitrary spatial frequency greater than $1/h$, $P_0 = P_\varphi(f_0)$, $R_{\max}$ is the maximum distance between a pair of SAR image pixels, and f_s the data sampling rate used in the derivation of (9). The validity of the former at low and high frequencies has been limited, since compliance outside these scales has actually not been observed in SAR data. Namely, (9) was verified for $R_{\max} = 50$ km and $f_\mathrm{s} = (1/160)$ m^{-1}. It is expected that, as spatial frequency decreases (below one cycle in several hundred kilometers), the delays become uncorrelated, and the PSD will tend to flatten. In [15], measurements of tropospheric wind-speed PSD were found to follow a $-5/3$ exponent power law up to scales of about 400 km. The behavior at high frequencies (above one cycle in tens of meters) is not of great concern due to the small amplitude of atmospheric disturbances as compared to other noise sources.

The power-law model (9) was observed in interferometric phase originally rather than in radar wave phase φ directly. However, a two-regime model is expected to hold for the phase of each SAR acquisition, φ_1 and φ_2, since these regimes correspond to the first two in (2), for which a physical interpretation

was given. Assuming the atmospheric state to be uncorrelated at the two acquisition times, it is expected for interferometric phase $\Delta\varphi = \varphi_1 - \varphi_2$ to comply to the same power-law model, since in this case, $P_{\Delta\varphi}(f) = P_{\varphi 1}(f) + P_{\varphi 2}(f)$.

III. Proposed Model

A. Derivation

The statistics of interest for the interferometric SAR applications aforementioned in Section I are the covariance $\mathrm{Cov}\{\delta_i, \delta_j\}$ and the variance $\mathrm{Var}\{\delta_i - \delta_j\}$, where $\delta_i = (\lambda/4\pi)\Delta\varphi_i$ represents the slant range atmospheric delay of the ith interferogram pixel. Assuming the atmospheric states at the interferometric pair acquisition times to be uncorrelated and a cosine mapping function [4], the sought quantities are related to the zenith delay structure functions at the two acquisition times, $D_{\tau 1}(R)$ and $D_{\tau 2}(R)$, by the following relations:

$$\begin{aligned}\mathrm{Cov}\{\delta_i, \delta_j\} &= \frac{m^2(\theta)}{2}\big(D_{\tau 1}(\infty) - D_{\tau 1}(R) \\ &\qquad + D_{\tau 2}(\infty) - D_{\tau 2}(R)\big) \\ \mathrm{Var}\{\delta_i - \delta_j\} &= m^2(\theta)\left(D_{\tau 1}(R) + D_{\tau 2}(R)\right) \\ m(\theta) &= 1/\cos\theta. \end{aligned} \tag{10}$$

In (10), subscripts 1 and 2 denote the acquisition time, θ is the mean radar angle of incidence between the two acquisitions, and R is the horizontal distance.

A closed form for $D_\tau(R)$, representing the one-way zenith delay structure function at a generic acquisition time, may be derived from the one-sided phase PSD in (9), using (8). For convenience in the mathematical derivation, the maximum distance between two image pixels $R_{\max}$ as well as the sampling frequency f_s, which appear in (9), will be set to infinity. The former assumption implies that the spectrum will not flatten for low spatial frequencies, which in turn implies an infinite variance for the atmospheric phase disturbance. This unphysical assumption however will be corrected for in the spatial domain, following an approach proposed in [11]. The latter assumption instead is expected to have little impact on the derivations, due to the low power levels associated with increasing spatial frequencies in comparison with thermal noise.

Inserting (9) into (8) yields the following, after a change of variables and reordering:

$$\begin{aligned} D_\tau(R) &= P_0 C_0 \left[C_1 I_1\left(\frac{R}{h}\right) R^{2/3} + C_2 I_2\left(\frac{R}{h}\right) R^{5/3} \right] \\ C_0 &= \left(\frac{\lambda}{4\pi}\right)^2 \quad [m^2] \\ C_1 &= 4 f_0^{8/3} \pi^{2/3} h \quad [m^{-5/3}] \\ C_2 &= 4 f_0^{8/3} \pi^{5/3} \quad [m^{-8/3}] \\ I_1\left(\frac{R}{h}\right) &= \int_0^{\pi R/h} u^{-5/3} \sin^2(u) du \\ I_2\left(\frac{R}{h}\right) &= \int_{\pi R/h}^{\infty} u^{-8/3} \sin^2(u) du. \end{aligned} \tag{11}$$

TABLE I
Structure-Function Model Parameters

Parameter	Value	Unit	Description
P_0	9.04	m	$P_\varphi(f_0)$
f_0	1	1 km^{-1}	arbitrary spatial frequency
L	2133	km	saturation scale length
h	3	km	tropospheric height
s	8	m/s	tropospheric wind speed
A_1	0.472	-	constant
C_3	1.4731	-	constant
A_2	0.466	-	constant
C_4	3.2177	-	constant

Parameter f_0 was chosen arbitrarily, whereas P_0=$P_\varphi(f_0)$ and L were computed solving (14) and (15), using 1 cm and 2.4 cm as the daily and annual rms of zenith atmospheric delay. Parameters h and s were assigned based on [13] and [11] respectively.

The computation of the earlier integrals may be done numerically; however, a closed form is of practical interest, and an accurate approximation is reported in

$$\begin{aligned} I_1\left(\frac{R}{h}\right) &= \begin{cases} \frac{3}{4}u^{4/3} - \frac{1}{10}u^{10/3}, & \frac{R}{h} \le A_1 \\ C_3 - \frac{3}{4}u^{-2/3}, & \frac{R}{h} > A_1 \end{cases} \\ I_2\left(\frac{R}{h}\right) &= \begin{cases} C_4 - 3u^{1/3} + \frac{1}{7}u^{7/3}, & \frac{R}{h} \le A_2 \\ \frac{3}{10}u^{-5/3}, & \frac{R}{h} > A_2. \end{cases} \end{aligned} \tag{12}$$

In (12), $u = \pi R/h$, and the values of the constants are shown in Table I. The accuracy of the closed-form approximation is further discussed in Section IV.

B. Convergence at Infinity

It has been pointed out in [11] that a power-law structure function leads to an unphysical feature at infinity, since tropospheric delay should be uncorrelated for two infinitely distant points. Following the approach of [11], a multiplying factor dependent on a saturation scale L is introduced to provide convergence of the structure function at infinity. The same factor used in [11] for the refractivity structure function is used here for the delay structure function, based on the proportionality of the two for $R \gg h$ discussed in Section II-A. Therefore, the model can be modified, leading to

$$D_\tau(R) = P_0 C_0 \left[\frac{C_1 I_1\left(\frac{R}{h}\right) R^{2/3}}{\left[1 + \left(\frac{R}{L}\right)^{2/3}\right]} + C_2 I_2\left(\frac{R}{h}\right) R^{5/3} \right]. \tag{13}$$

For SAR applications, the scales of interest are typically $R < 400$ km. For these distances, (13) is based on the InSAR observations which lead to (9) and on the assumption that the first regime in (9) still holds for $R \ll L$, which is in agreement with [15]. At greater distances, (13) is not supported by observations and, actually, contradictions arise with those in [15]. In order to extend (9) and, thus, (13), tropospheric delay signal should be isolated in InSAR data at these scales. This is not a trivial task, due to SAR processing issues (handling of Doppler centroid and baseline variations), ionospheric effects, and the large data volumes involved and would be useful only for a limited amount of SAR applications. Therefore, it is considered outside the scope of this letter.

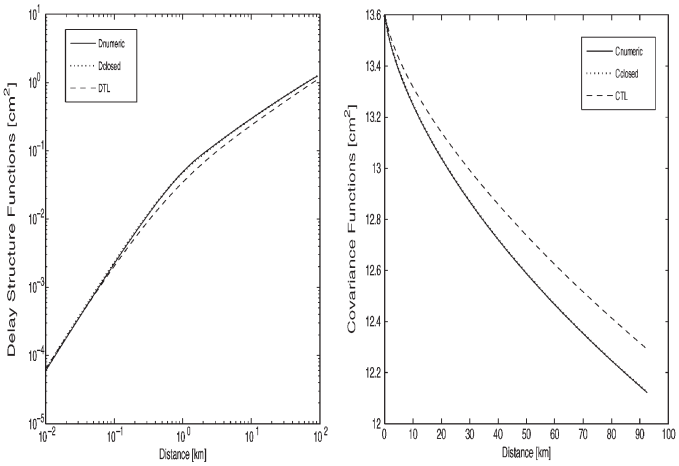

Fig. 1. (Left) Closed-form and numeric delay structure functions derived in this letter (continuous and dotted line, respectively) as compared to that of [11] (dashed line). (Right) Corresponding interferogram path-length covariances (10) assuming similar atmospheric state at the two acquisitions.

C. Tuning of Model Parameters

In order to use the delay structure function model (13), parameters P_0 and L must be computed. In the absence of any scene-specific information concerning the power of the atmospheric disturbance, published atmospheric delay statistics may be used. Assuming ergodicity and that the spatial structure of the turbulence is "frozen" and moves with a constant wind speed s, spatial and temporal statistics may be interchanged so that distance R corresponds to st, where t is the time variable. Measured delay variances over a time T and the model expressions (13) and (12) can then be used to setup two equations in the two unknowns P_0 and L as follows [11]:

$$\lim_{R\to\infty} D_\tau(R) = 2\cdot \mathrm{Var}\{\tau\} \simeq 2\cdot \sigma_\tau^2(T)|_{T=1\ \mathrm{year}} \qquad (14)$$

$$\frac{1}{T^2}\int_0^T (T-t) D_\tau(R)|_{R=st} dt = \sigma_\tau^2(T)|_{T=24\ \mathrm{h}}. \qquad (15)$$

A finite long-term (long-distance) variance is enforced by (14), and its left-hand side may be represented in closed form using (13) and solved for L (for a given P_0), leading to

$$L = \left(\frac{1}{C_1 C_3}\left[\frac{2\cdot \mathrm{Var}\{\tau\}}{P_0 C_0} - 0.3\cdot C_2 \left(\frac{h}{\pi}\right)^{5/3}\right]\right)^{3/2}. \qquad (16)$$

A measured long-term variance (annual for example) may be used for $\mathrm{Var}\{\tau\}$. Equation (16) enforces agreement with a second (short-term) variance measurement, and since a closed form is quite lengthy, its left-hand side is more conveniently computed numerically and solved for P_0 (for a given L). Equations (15) and (16) can be solved iteratively, initializing L to the 3000-km value reported in [11] and using globally representative values for the long- and short-term variances, although, strictly speaking, these are latitude- and season-dependent quantities [15]. Physically reasonable values for P_0 are expected to range from 1 to 40 m, according to the observations of [1], whereas L should be between 2000 and 3000 km according to [10].

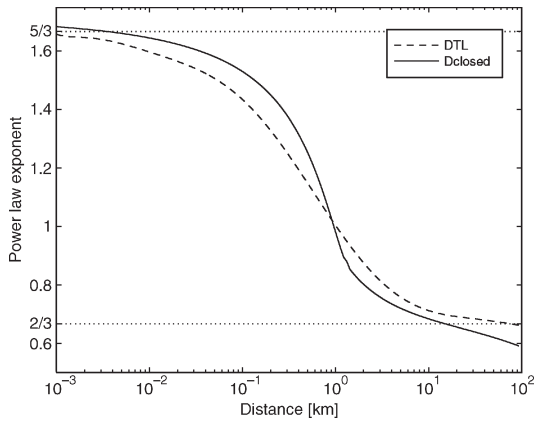

Fig. 2. Exponents from local power-law fits to the structure function curves in Fig. 1 versus distance R.

Should a PSD measurement at a certain spatial frequency be available at an acquisition time, this would provide a value for P_0 in (13), and L could be computed from (16). Therefore, in (10), $D_{\tau 1}(R)$ and $D_{\tau 2}(R)$ may, in general, have a $P_{01} \neq P_{02}$ and an $L_1 \neq L_2$, whereas $D_{\tau 1}(\infty) = D_{\tau 2}(\infty) = 2\mathrm{Var}\{\tau\}$.

External sources, which should be investigated to tune P_0, are high-resolution numerical weather models as well as satellite spectrometer and radiometer data.

IV. Comparison With Previously Published Results

A closed-form model was obtained, tuning the free parameters (P_0, L) in (13), to globally representative atmospheric statistics, using (14) and (15). The expressions reported in (12) were used. For comparison, a model was also derived, with integrals I_1 and I_2 evaluated numerically. The model parameters h and s were, in both cases, set to 3 km [13] and 8 m/s [11], respectively. The procedure outlined in the previous section was used to compute P_0 and L, using 1 and 2.4 cm as the measured daily and annual rms of atmospheric delay [11]. A list of all model parameters is shown in Table I. The reported P_0 and L values are those of the closed-form model, which differ only slightly from those computed for the numerical one.

A first comparison between the numerical and the closed-form structure functions derived in this letter is shown in Fig. 1. The relative error, due to the approximations used in deriving (12), amounts to less than 5% and causes an error of less than 0.1% in the interferometric path length covariance. The former was computed through (10), assuming similar atmospheric state at the two acquisitions. These error figures are negligible for applications, and in the following, only the closed-form model shall be considered.

Second, the closed-form structure function of this letter was compared that of the work of Treuhaft and Lanyi [11], plotted as a dashed line in Fig. 1 (left). The greatest relative difference is observed around $R = h$ and amounts to about 30%, whereas the corresponding difference in interferometric path-length covariance grows to 1.5% over a 100-km distance. The observed differences are imputable to the piecewise approximation of the PSD in (9), used to derive the model of this letter, as well as to the different values of h chosen (3 km in this letter as opposed to 1 km in [11]). These factors influence the exponent of the

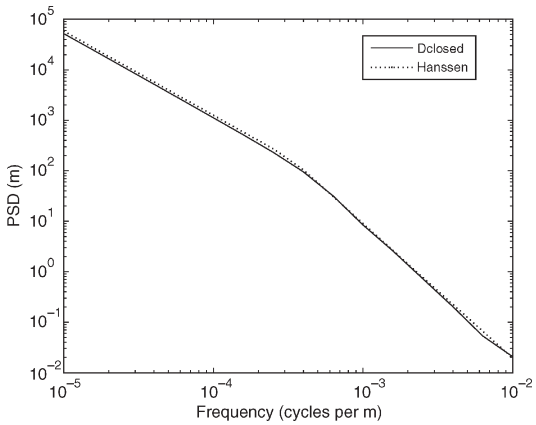

Fig. 3. PSD of radar phase computed from the closed-form structure function (continuous line) of this letter and (dotted line) from (9).

local power-law fit to the structure function models, as shown in Fig. 2. It may also be noted from Fig. 2 that over a 100-km range, the power-law exponent in (13) varies continuously from 5/3 to 2/3, in agreement with (2).

A third comparison was carried out in the spatial frequency domain. The phase PSD corresponding to (13) was computed using the values in Table I and is shown in Fig. 3 together with (9). These spectrums are expected to differ due to the denominator in (13), which is introduced to flatten the PSD at low frequencies. However, over typical SAR image scales, the relative differences were found to be below 15%. Considering the uncertainties in the scene-dependent model parameters h, s, and P_0, it may be assumed for all practical purposes that parameter P_0 in (13) still represents the corresponding PSD at $f = f_0$.

Finally, the P_0 value derived in this letter (Table I) was compared to the values reported in [1], representative of a variety of weather conditions. The following equation may be used to compare these values:

$$P_{0H} = 2f_{\mathrm{s}} \left(\frac{\lambda}{4\pi \cos\theta_0} \right)^2 P_0 \tag{17}$$

where P_{0H} represents the PSD at frequency f_0 of the interferometric path-length delay, reported in [1, p. 143], whereas P_0 represents the single-acquisition-phase PSD at frequency f_0, which appears in (13). The other parameters are the data-sampling frequency f_{s} and the nominal ERS incidence angle θ_0 and wavelength λ. The formula is based on the discrete equivalent of (5), since the PSDs in [1] were computed from interferograms and assumes the same power of the atmospheric disturbance in the two acquisitions. Substituting $f_{\mathrm{s}} = (1/160)$ m^{-1} [13, p. 28], $\lambda = 5.6$ cm, $\theta_0 = 23^\circ$, and $P_0 = 9$ m from Table I, we obtain $P_{0H} = 2.7$ mm^2. This represents a median value for the observations reported in [1], which, overall, ranged from 0.3 to 11.2 mm^2.

V. Conclusion

A model for the second-order statistics of the propagation delay associated with spatiotemporal refractivity fluctuations in the troposphere was derived. A closed-form expression for the zenith delay structure function was obtained from a two-regime PSD function reported in the literature [1], [13], the validity of which is limited to typical SAR scales (< 400 km). The underlying assumptions are wide-sense stationarity and circular symmetry of the considered process. The model contains four independent parameters, namely, effective tropospheric height, effective wind speed, correlation distance, and the PSD at a given spatial frequency.

The first two parameters are considered fixed, whereas the latter two may be computed exploiting acquisition-specific information, as well as "off-the-shelf" tropospheric-delay statistics. For their estimation, in the absence of any scene-specific information, globally representative measures of the daily and annual variances of tropospheric delay are required to set up a system of two equations in the two unknowns. However, should a PSD measurement at a single spatial frequency be available at each image acquisition time, this would provide scene-specific equations the model could exploit.

Future improvements should address the modeling of vertical-stratification variations and parameter tuning using external data sources.

References

[1] R. F. Hanssen, *Radar Interferometry: Data Interpretation and Error Analysis*. Dordrecht, The Netherlands: Kluwer, 2001.

[2] J. J. Mohr and J. P. Merryman Boncori, "A framework for error prediction in interferometric SAR," in *Proc. ENVISAT Symp.*, Montreaux, Switzerland, Apr. 2007, pp. 23–27. ESA SP-636.

[3] T. R. Emardson, M. Simons, and F. H. Webb, "Neutral atmospheric delay in interferometric synthetic aperture radar applications: Statistical description and mitigation," *J. Geophys. Res.*, vol. 108, no. B5, 2231, 2003.

[4] S. Williams, Y. Bock, and P. Fang, "Integrated satellite interferometry: Tropospheric noise, GPS estimates and implications for interferometric synthetic aperture radar products," *J. Geophys. Res.*, vol. 103, no. B11, pp. 27 051–27 067, 1998.

[5] Z. Li, J. P. Muller, P. Cross, and E. J. Fielding, "Interferometric synthetic aperture radar (InSAR) atmospheric correction: GPS, Moderate Resolution Imaging Spectroradiometer (MODIS), and InSAR integration," *J. Geophys. Res.*, vol. 110, no. B3, B03 410, 2005.

[6] Z. Li, E. J. Fielding, P. Cross, and J. P. Muller, "Interferometric synthetic aperture radar atmospheric correction: Medium resolution imaging spectrometer and advanced synthetic aperture radar integration," *Geophys. Res. Lett.*, vol. 33, no. L6, p. L06 816, 2006.

[7] Z. Li, E. J. Fielding, P. Cross, and J. P. Muller, "Interferometric synthetic aperture radar atmospheric correction: GPS topography-dependent turbulence model," *J. Geophys. Res.*, vol. 111, no. B2, B02 404, 2006.

[8] V. I. Tatarski, *Wave Propagation in Turbulent Medium*. New York: McGraw-Hill, 1961. (cit. in [1]).

[9] C. E. Coulman and J. Vernin, "Significance of anisotropy and the outer scale of turbulence for optical and radio seeing," *Appl. Opt.*, vol. 30, no. 1, pp. 118–126, Jan. 1991.

[10] A. A. Stotskii, "Concerning the fluctuation characteristics of the earth's troposphere," *Radiophys. Quantum Electron.*, vol. 16, no. 5, pp. 620–622, May 1973. (translated from Russian).

[11] R. N. Treuhaft and G. E. Lanyi, "The effect of the dynamic wet troposphere on radio interferometric measurements," *Radio Sci.*, vol. 22, no. 2, pp. 251–265, Mar. 1987.

[12] R. Hannsen, A. Ferretti, M. Bianchi, R. Grebenitcharsky, F. Kleijer, and A. Elawar, "APS estimation and modeling for radar interferometry," in *Proc. Fringe*, 2005. [Online]. Available: http://earth.esa.int/fringe2005/proceedings/

[13] R. F. Hanssen, D. N. Moisseev, and S. Businger, "Resolving the acquisition ambiguity for atmospheric monitoring in multi-pass radar interferometry," in *Proc. IGARSS*, Toulouse, France, Jul. 21–25, 2003, pp. 1202–1205.

[14] R. F. Hanssen, "Atmospheric heterogeneities in ERS tandem SAR interferometry," Delft Univ. Press, Delft, The Netherlands, DEOS Rep. 98.1, 1998.

[15] F. A. Gifford, "A similarity theory of the tropospheric turbulence energy spectrum," *J. Atmos. Sci.*, vol. 48, no. 8, pp. 1370–1379, Apr. 1988.